Title

Crystallization and preliminary X-ray diffraction study of the ligand-binding domain of the bacterial chemotaxis-mediating aspartate receptor of Salmonella typhimurium.

Journal

Journal of molecular biology, 221(1)

ISSN

0022-2836

Authors

Jancarik, J
Scott, WG
Milligan, DL
et al.

Publication Date

1991-09-01

DOI

10.1016/0022-2836(91)80198-4

Peer reviewed

J. Mol. Biol. (1993) **232**, 555–573

Refined Structures of the Ligand-binding Domain of the Aspartate Receptor from *Salmonella typhimurium*

William G. Scott[1], Daniel L. Milligan[2]†, Michael V. Milburn[1]‡ Gilbert G. Privé[1]§, Joanne Yeh[1], Daniel E. Koshland, Jr[2] and Sung-Hou Kim[1]

[1]*Department of Chemistry and Lawrence Berkeley Laboratory University of California, Berkeley, CA 94720, U.S.A.*

[2]*Department of Molecular and Cellular Biology University of California, Berkeley, CA 94720, U.S.A.*

(Received 27 October 1992; accepted 16 March 1993)

The aspartate receptor is a transmembrane-signalling protein that mediates chemotaxis behaviour in bacteria. Aspartate receptors in *Salmonella typhimurium* and *Escherichia coli* exist as dimers of two subunits in the presence as well as in the absence of aspartate. We have previously reported the three-dimensional structures of the external ligand-binding domain of the *S. typhimurium* aspartate receptor with and without bound aspartate. The external or periplasmic region of the aspartate receptor is a dimer of four-α-helical bundle subunits; a single aspartate molecule binds to one of two sites residing at the subunit interface, increasing the affinity of the subunits for one another.

Here we report the results of a detailed analysis of the aspartate receptor ligand-binding domain structure (residues 25 to 188). The dimer interface between the twofold related subunits consists primarily of contacts mediated by the side-chains of the N-terminal helix of each four-α-helical bundle subunit. The N-terminal helices pack approximately 20° from parallel as an approximate coiled-coil super-secondary structure.

We have refined aspartate receptor ligand-binding domain structures in the presence and in the absence of a bound aromatic compound, 1,10-phenanthroline, to 2·2 Å and 2·3 Å resolution, respectively, as well as crystal structures in the presence of specifically bound Au(I), Hg(II) and Pt(IV) complex ions at 2·4 Å, 3·0 Å and 3·3 Å resolution, respectively. The possible biological relevance of the aromatic ligand-binding site and the metal ion-binding sites is discussed.

The dimer of four-α-helical bundle subunits composing the periplasmic region of the *S. typhimurium* aspartate receptor provides a basis for understanding the results of mutational analyses performed on related chemotaxis transmembrane receptors. The crystal structure analysis provides an explanation for the way in which mutations in the *E. coli* aspartate receptor affect its binding to the periplasmic maltose-binding protein and how mutations in the more distantly related *E. coli* Trg chemotaxis receptor affect its binding to the periplasmic ribose and glucose-galactose binding proteins.

Keywords: receptor; structure; chemotaxis; transmembrane; ligand-binding

1. Introduction

Signal transduction is most commonly initiated by a ligand molecule binding to its transmembrane receptor protein residing on the cell surface. Ligand-binding results in the transmission of information from the outside to the inside of the cell. Included among the various morphologies of transmembrane receptors are two families that share a common structural motif: an extracellular ligand-binding domain coupled to an intracellular signalling domain by one or two transmembrane sequences. One family that has a single transmembrane domain per subunit includes the struc-

† Present address: Howard Hughes Medical Institute, University of California, San Francisco, CA 94143, U.S.A.

‡ Present address: Howard Hughes Medical Institute, Childrens Hospital, Boston, MA 02115, U.S.A.

§ Present address: Molecular Biology Institute, University of California, Los Angeles, CA 90024, U.S.A.

0022-2836/93/140555-19 $08.00/0

turally homologous eukaryotic growth-factor receptors (Ullrich & Schlessinger, 1990; Hanks *et al.*, 1988; Yarden & Ullrich, 1988) of insulin (Ullrich *et al.*, 1985), insulin-like growth-factor (Ullrich *et al.*, 1986), epidermal growth-factor (Ullrich *et al.*, 1984), nerve growth-factor (Parada, 1991), platelet-derived growth factor (Claesson-Welsh, 1988) and colony stimulating factor 1 (Coussens *et al.*, 1986); all possess tyrosine kinase activity in the signalling or effector domain. The other family includes the receptors having two transmembrane sequences that mediate bacterial chemotaxis in *Escherichia coli* and *Salmonella typhimurium*, such as the aspartate receptor (Russo & Koshland, 1983), the serine receptor (Krikos *et al.*, 1983) and the receptor for ribose-galactose-binding proteins, Trg (Harayama *et al.*, 1982). Although much has been learned from gene sequencing and biochemical studies of these and other receptor proteins, the fundamental mechanism of transmembrane signalling remains unknown.

The chemotaxis-mediating receptors of *E. coli* and *S. typhimurium* allow these bacteria to sense and respond to gradients of chemical attractants or repellents (Adler, 1966; Macnab, 1987). In the presence of attractant molecules such as aspartate, bacteria alter their random motion and migrate toward the source of the attractant. Thus, bacterial chemotaxis receptors form an integral part of a simple memory system that enables bacteria to exhibit behavioural responses that optimize their chances of survival (Macnab & Koshland, 1972; Macnab, 1987; Koshland, 1988). Two different mechanisms constitute this memory: a fast excitation process and a slower adaptation process (Macnab & Koshland, 1972). The fast excitation process involves a series of phosphorylation events catalyzed by the soluble cytoplasmic kinase chemotaxis enzyme CheA (Bourret *et al.*, 1989). The slower adaptation process involves a series of methylations and demethylations (Adler, 1966) of the effector domain of the receptor catalyzed by the soluble methyltransferase CheR and the phosphorylated methylase CheB, respectively (Weis & Koshland, 1988). These two processes function in concert to coordinate a comparison of past and present conditions outside of the cell (Macnab & Koshland, 1972; Segall, *et al.*, 1986) resulting in a fine-tuned chemotaxis response. The biochemistry of bacterial chemotaxis has been the subject of several recent and detailed reviews (Macnab, 1987; Koshland, 1988; Stock, *et al.*, 1990. Bourret, *et al.*, 1991; Stock *et al.*, 1992).

The aspartate receptor is the best understood of the chemotaxis receptors. The exterior periplasmic domain contains the aspartate-binding site and the interior cytoplasmic effector domain contains the sites for methylation and activation of the phosphorylation events (Russo & Koshland, 1983; Mowbray *et al.*, 1985). Analysis of conserved features within the eukaryotic growth-factor receptor family (Hanks *et al.*, 1988) suggests that these transmembrane receptors share a similar architecture to that of the chemotaxis receptors and thus may also share a common mechanism of signal transduction. Construction of a functionally active chimeric transmembrane receptor consisting of the ligand-binding domain and transmembrane sequences of the aspartate receptor coupled to the cytoplasmic portion of the insulin receptor tyrosine kinase domain strongly suggests that a common mechanism is indeed responsible for transmembrane signalling in both types of receptors (Moe *et al.*, 1989). The aspartate receptor (Milligan & Koshland, 1988) exists as a dimer both in the absence and in the presence of its ligands, indicating that the postulated common mechanism of transmembrane signalling involves a conformational change within the dimeric protein. Crosslinking studies have provided evidence of such a conformational change in the case of the aspartate receptor (Falke & Koshland, 1987).

Sequence analyses and biochemical studies implicate a threonine residue at position 154 (Lee & Imae, 1990) as well as three arginine residues, at positions 64, 69 and 73, in the periplasmic domain (Wolff & Parkinson, 1988; Mowbray & Koshland, 1990) as critical for aspartate binding. Two glutamate and two glutamine residues at positions 302, 491. 295 and 309, respectively, are the methylation sites in the cytoplasmic effector domain (Terwilliger *et al.*, 1986). Elucidation of transmembrane signalling would be greatly facilitated by determining the three-dimensional crystal structure of the intact aspartate transmembrane receptor in both the liganded and unliganded states. Unfortunately, integral membrane proteins are notoriously difficult to crystallize (Garavito & Picot, 1990) and the aspartate receptor is no exception. Because attempts to produce diffraction-quality crystals of the intact receptor for X-ray crystallography have so far been unsuccessful, we decided to approach this problem by determining the structure of the receptor piecewise. A similar approach has recently yielded the structure of the human growth hormone complexed to the extracellular domain of its receptor (de Vos *et al.*, 1992).

We have been able to obtain high-quality crystals of a functional cysteine-crosslinked dimer of the ligand-binding domain (residues 25 to 188) of the aspartate receptor in both the absence and the presence of bound aspartate (Jancarik *et al.*, 1991). Here, we report five refined structures of the ligand-binding domain in the absence of aspartate. These structures include a 2·2 Å resolution structure of the domain in the presence of the aromatic ligand 1,10-phenanthroline, a 2·3 Å resolution structure of the same protein but in the absence of phenanthroline, as well as 2·4 Å, 3·0 Å and 3·3 Å resolution structures of the protein in the absence of phenanthroline but in the presence of specifically bound Au(I), Hg(II) and Pt(IV) metal complex ions.

Here, we present an analysis of these five refined crystal structures of the ligand-binding domain of the aspartate receptor and we discuss the possible biological relevance of the aromatic ligand-binding

site and of the metal ion-binding sites as well as their implications for signal transduction. The results of our crystal structure analyses on the ligand-binding domain allow us to infer the corresponding structures of the other members of the chemotaxis transmembrane receptor family. To illustrate the veracity of this inference, we show how mutations in the *E. coli* aspartate receptor that affect its binding to the periplasmic maltose-binding protein and how mutations in the more distantly related *E. coli* Trg chemotaxis receptor that affect its binding to the periplasmic ribose and glucose-galactose binding proteins may be understood on the basis of our *S. typhimurium* aspartate receptor crystal structure.

2. Materials and Methods

(a) *Preparation and crystallization*

Preparation procedures and crystallization conditions of the ligand-binding domain of the aspartate receptor are reported elsewhere (Milligan, 1991; Jancarik *et al.*, 1991). The sequence of the receptor fragment we crystallized starts with methionine 25 (changed from serine 25 in the wild-type receptor) and ends with arginine 188. Because crystals of the wild-type periplasmic domain diffracted poorly, we have employed a cysteine 36 mutant disulfide-crosslinked dimeric form of the periplasmic domain, corresponding to a biologically active (as assayed by the enhanced methylation rate of the cytoplasmic domain upon aspartate binding) intact asparagine 36 to cysteine 36 mutant receptor (Falke & Koshland, 1987) crosslinked as a disulfide-bonded dimer, for our crystallographic analyses.

We obtained high-quality single crystals of the cysteine 36 mutant crosslinked aspartate receptor periplasmic domain in the absence of aspartate in 0·1 M Hepes (pH 7·4), 1·5 M Li_2SO_4 sitting drops as previously described (Jancarik *et al.*, 1991). We initially added 0·5 mM Cu(II)[1,10-phenanthroline] as an oxidizing agent to maintain the disulfide crosslink because a contaminant (most likely traces of Fe(II) in commercially prepared Li_2SO_4) inhibited crystallization by reducing the disulfide crosslink. Subsequently we found 0·5 mM EDTA served equally well to protect the disulfide bond from reduction (presumably by sequestering Fe(II) ions). In both cases hexagonal crystals having the space group $P6_522$ with cell dimensions $a = b = 80{\cdot}03$ Å, $c = 155{\cdot}6$ Å formed within days. One subunit of the cysteine 36 crosslinked dimer of the periplasmic domain resides in an asymmetric unit of the crystal.

(b) *Acquisition of diffraction data*

Diffraction data to 2·2 Å resolution for the native protein crystal (which would later prove to be a complex with the aromatic ligand phenanthroline) as well as anomalous scattering data to 2·3 Å resolution for the $KAu(CN)_2$ isomorphous derivative were collected on Fuji type II phosphor imaging plates using 1·0 Å X-rays at the Photon Factory in Tsukuba, Japan, and were processed as described (Milburn *et al.*, 1991). A 2·3 Å data set for a second native protein crystal (formed in the absence of phenanthroline) was subsequently collected on phosphor imaging plates on an R-Axis II rotation camera using a conventional rotating anode X-ray source at 1·54 Å. The data were similarly processed with R-axis II software (Molecular Structure Corporation, 1991; Rossmann, 1979). Additional heavy-atom derivative data sets, including $K_2Hg(SCN)_4$ and $K_2Pt(SCN)_6$, were collected on film at a wavelength of 1·54 Å using an Enraf-Nonius rotation camera at the Stanford Synchrotron Radiation Laboratory. The films were digitized using a drum scanner (Optronix Corp) and the data were processed using computer programs originally written by Rossmann (1979). Reflection data were merged and scaled using the crystallographic program package PROTEIN (Steigemann, 1982). Data collection results and reduction statistics for the native crystals and the heavy-atom derivatives are summarized in Table 1.

(c) *Structural determination*

Difference Patterson maps were calculated for all derivatives using diffraction data ranging between 10 Å and 3 Å resolution and were interpreted for heavy-atom positions with the use of the program HASSP (Terwilliger *et al.*, 1987). An anomalous difference Patterson map was calculated for the Au derivative and similarly interpreted. The Au and Hg isomorphic difference Pattersons each revealed 2 sites (Table 2) as 2 single-site solutions in the difference Patterson maps. The Au anomalous difference Patterson confirmed the 2 Au sites and revealed a strong cross-peak, thereby confirming that a strong anomalous signal was present in the Au derivative data. The Pt derivative did not yield a readily interpretable Patterson map and therefore was not used to calculate phases. Multiple isomorphous replacement (MIR†) with anomalous scattering phase refinement was carried out using PROTEIN as described (Milburn *et al.*, 1991). The derivative phase refinement statistics are shown in Table 2. The heavy-atom refinement parameters, including co-ordinates, temperature factors, relative occupancies and scaling *R*-factors, are reported in Table 3.

A total of 154 amino acid residues was initially assigned to the electron density within 1 asymmetric unit of the crystal, starting with methionine 25 and ending at phenylalanine 180, as described in Results, section (a). (Fig. 1). The last 8 amino acid residues were disordered. Immediately apparent from observation of the crystal packing contacts is the fact that the periplasmic domain of the receptor is a dimer in which the crystallographic twofold axis is coincident with that of the dimer of receptor subunits (Fig. 2). Further results of the structural determination are reported by Milburn *et al.* (1991), and in Results.

(d) *The crystal structure refinements*

The initial aspartate receptor periplasmic domain structure (residues 25 to 180), constructed using the graphics display program FRODO (Jones, 1978), was subsequently refined using the simulated annealing program in XPLOR 2.1 (Brünger, 1990) incorporating a slow-cooling protocol. Initially using 8·0 to 2·4 Å resolution data and a starting temperature of 4000 K, 50 cycles of refinement at 0·5 fs steps/100 K decrease in temperature were performed followed by 120 cycles of conjugate gradient energy minimization, yielding an *R*-factor of 27% with the overall temperature factor set at 20·0 Å^2. Individual temperature factors were then refined before calculation

† Abbreviation used: MIR, multiple isomorphous replacement; r.m.s., root-mean-square.

Table 1
Data collection and processing statistics

Crystal	Derivative conditions	Number of measurements	Number of reflections†	Completeness (%)†	R_{merge} (%)	Resolution (Å)
Native with phenanthroline		83,066	12,087	76·9	6·99	2·2
Native without phenanthroline		78,456	11,273	79·2	6·80	2·3
$KAu(CN)_2$ derivative	20 mM 12 h	72,346	8941 (14,615)‡	83·4	8·62 5·21§	2·4
$K_2Hg(SCN)_4$ derivative	1·0 mM 2 h	28,279	5434	83·4	9·50	3·0
$K_2Pt(SCN)_6$ derivative‖	2·0 mM 6 h	24,876	4358	89·1	10·5	3·3

† These figures are for the data actually used in the structural refinements, i.e. with a 6·0 Å low-resolution cutoff (or 8·0 Å cutoff in the case of Hb and Pt) and a $F > 2\sigma$ cutoff.

‡ Anomalous scattering data were collected on the Au derivative. The number in parentheses includes all measured Bijvoet pairs.

§ Overall average Bijvoet pair differences due to anomalous scattering effects.

‖ This derivative was not used to calculate phases.

$$R_{merge} = 100 \times \sum_{hkl} \sum_{i} \frac{|\langle I(hkl)\rangle - I_i|}{\langle I(hkl)\rangle}.$$

of electron density maps. The refined structure was inspected against Sim-weighted (Sim, 1960) $2F_{obs}-F_{calc}$ and MIR electron-density maps and was adjusted manually using the graphics display program FRODO. After several cycles of simulated annealing, conjugate gradient minimization, and temperature factor refinement followed by manual adjustment of the protein model to the electron density, an *R*-factor of 20·7% to 2·4 Å resolution data using a total of 8745 reflections greater than 2σ was obtained (Milburn *et al.*, 1991).

(i) *The 2·2 Å structure in the presence of an aromatic ligand*

Refinement of the original aspartate receptor periplasmic domain crystal structure in the absence of aspartate was then continued using all 11,254 reflections with *F* values greater than 2σ and between 6·0 and 2·2 Å resolution. The first cycle of simulated annealing, conjugate gradient minimization, and temperature factor refinement produced an *R*-factor of 24·1%. At this point electron density situated between the N terminus and the disulfide crosslink corresponding most closely to a 3-ring planar aromatic molecule of mm2 symmetry was quite pronounced in a difference Fourier ($F_{obs}-F_{calc}$) electron density map contoured at 3σ as shown in Fig. 3. 1,10-Phenanthroline was judged to be the most likely candidate for the molecule corresponding to this electron density, as it possessed the required geometry and was present in the crystallization mixture (see above). Phenanthroline was thus built into the model such that its twofold symmetry axis was coincident with that of the crystal (Fig. 2(b)). Two more cycles of simulated annealing, conjugate gradient minimization, and temperature factor refinement, combined with manual adjustment of the phenanthroline and surrounding residues, produced an *R*-factor of 22·7. Water molecules were identified using difference Fouriers contoured at 3σ as peaks located close to possible hydrogen-bond donors or acceptors belonging to the protein molecule and the phenanthroline ligand. Sim-weighted (Sim, 1960) $2F_{obs}-F_{calc}$ and $3F_{obs}-2F_{calc}$ maps as well as a difference Fourier map calculated from the structure omitting residues 77 through 87 (the disordered loop 1) in the refinement and map calculation revealed no improvement in the density of this region. Therefore, residues 77 through 87 of this disordered loop were omitted from our model of the final structure. However, density corresponding to residues 181 to 184 (absent in the initial model) of the disordered C terminus of the receptor fragment emerged at the final stages of refinement, and these residues were thus included in the final model. The results of the refinement are described in Results.

(ii) *The 2·3 Å structure in the absence of phenanthroline*

Once it became apparent that phenanthroline was bound to the original native crystal, a second native dataset was collected on a crystal grown in the absence of the copper-phenanthroline complex but in the presence of

Table 2
MIR phase calculation and refinement statistics

	Resolution (Å)	10·0–7·7	7·7–6·3	6·3–5·3	5·3–4·6	4·6–4·0	4·0–3·6	3·6–3·3	3·3–3·0	Total
	$\langle m \rangle$	0·59	0·58	0·65	0·67	0·66	0·63	0·60	0·52	**0·60**
$KAu(CN)_2$	*Fh/E*	2·17	2·28	2·57	2·04	1·44	1·56	1·74	1·67	**1·93**
	*R*cullis	0·52	0·53	0·50	0·56	0·69	0·61	0·60	0·60	**0·59**
	*R*factor anomalous	0·53	0·57	0·50	0·45	0·35	0·48	0·53	0·68	**0·53**
$K_2Hg(SCN)_4$	*Fh/E*	1·13	1·22	1·19	1·03	0·84	0·87	0·83	0·81	**0·95**
	*R*cullis	0·68	0·63	0·65	0·65	0·66	0·64	0·66	0·65	**0·65**

Table 3
Heavy-atom parameters from the 3·0 Å MIR phasing

Derivative	Site	Orthogonal co-ordinates (Å) X	Y	Z	Occupancy	(Å)^2 Temp. factor	R_{scale} %
Au	1	13·734	40·843	161·896	1·00	50·77	24·3
	2	25·675	40·120	161·848	0·49	24·96	
Hg	1	−3·206	56·177	176·205	0·69	56·51	18·6
	2	18·942	36·301	165·506	0·39	40·10	

$$R_{scale} = 100 \times \frac{\sum_{hkl} |F_{native}(hkl) - F_{derivative}(hkl)|}{\sum_{hkl} |F_{native}(hkl)|}.$$

EDTA. Using the 2·4 Å refined structure described in section (c), above (but omitting residues 77 to 87 of loop 1), 2 cycles of simulated annealing, conjugate gradient minimization, and temperature factor refinement, combined with manual adjustment of several side-chains (most notably Phe40 and Phe180) near the phenanthroline-binding site, produced a refined structure using all 10,411 reflections with F values greater than 2σ and between 6·0 and 2·3 Å resolution. The results of this refinement are reported in Results. The absence of bound phenanthroline was confirmed by calculating a difference Fourier. No electron density was present in the phenanthroline binding site in a difference Fourier contoured at 1·0 σ; thus, no other molecule appeared to bind at this site in the absence of phenanthroline.

(iii) *Refinement of Au, Hg and Pt derivative structures*

Using the 2·4 Å refined structure described in section (c), above (but omitting residues 77 to 87 of loop 1), once again, 2 cycles of simulated annealing, conjugate gradient minimization and temperature factor refinement were performed upon each of the heavy-metal derivative structures in parallel. Heavy-metal binding sites were verified using difference Fouriers contoured at 5σ. The metal ions were then included in a subsequent round of refinement. The results of these refinements are summarized in Results. Due to the intermediate resolution of the Hg and Pt data, water molecules were not included in the refinement of these structures.

3. Results

(a) *Structural determination by multiple isomorphous replacement*

The solvent-flattened and phase-extended MIR electron density map calculated at 2·7 Å resolution was readily interpretable. For example, Figure 4 depicts electron density in an aromatic side-chain-rich region of the protein that was later found to bind 1,10-phenanthroline. The electron density map clearly revealed a cluster of four α-helices, which are depicted schematically in Figure 1. The handedness of these helices confirms the space group to be $P6_522$ rather than $P6_122$. Two of the helices were clearly parallel to one another and antiparallel to the two others, thus restricting the possible connections between secondary structural elements of the protein. The electron density also revealed the location of many of the side-chains unambiguously, thus confirming that our polypeptide chain tracing was correct.

(b) *Refinement of the ligand-binding domain isostructures*

The final model structure consists of residues 25 to 76 and 88 to 184 of the aspartate receptor subunit (i.e. loop 1 was omitted), 127 water molecules and one-half of the phenanthroline ligand bound to each receptor ligand domain subunit and has an

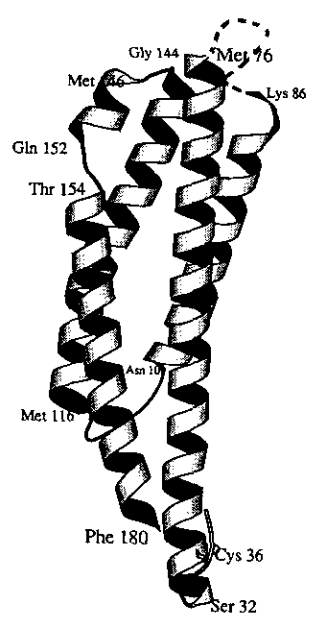

Figure 1. Ribbon diagram (Kraulis, 1991) of the aspartate receptor ligand-binding domain illustrating the connectivity of the 4-α-helix bundle. The beginning and ending residues of each helix are labelled, as is the cysteine residue at position 36 (whose side-chain is represented as a ball-and-stick model). Loop 1, which connects the N-terminal helix 1 to helix 2, is found to be disordered in the crystal structure and is thus represented as a broken line.

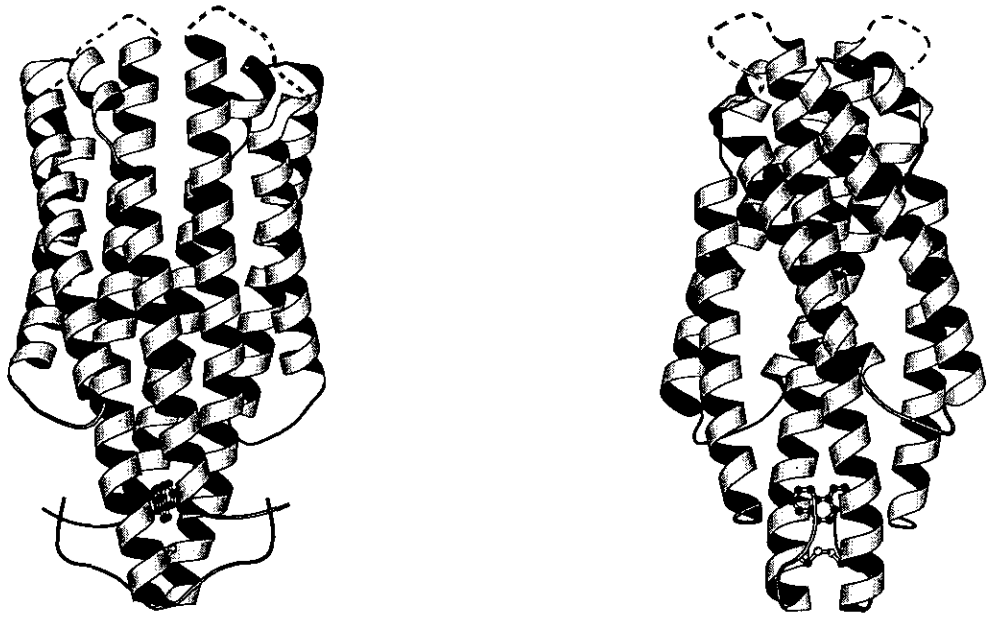

(a) (b)

Figure 2. (a) Ribbon diagram (Kraulis, 1991) illustrating the dimer of 4-α-helix bundles that constitutes the functionally active form of the aspartate receptor ligand-binding fragment. Loop 1 (residues 77 to 86), which connects helix 1 to helix 2, is quite disordered and is thus represented by broken lines. The primary side-chain interactions responsible for mediating the contacts between helices within the subunit are listed in Table 5, and those that mediate contacts between the monomers are listed in Table 6. The cysteine 36—cysteine 36′ disulfide crosslink and the bound aromatic ligand 1,10-phenanthroline are represented as ball-and-stick figures. (b) Ribbon diagram (90° rotation of (a)) illustrating more clearly the cysteine 36 disulfide crosslink and the bound phenanthroline.

Table 4
Refinement statistics

Data set	Native with phenanthroline	Native without phenanthroline	Au derivative	Hb derivative	Pt derivative
Resolution range (Å)	6·0–2·2	6·0–2·3	6·0–2·4	8·0–3·0	8·0–3·3
Number of reflections used $F > 2\sigma$	11,254	10,403	13,340†	5120	5436
R-factor (%)	18·8	20·9	20·2	20·9	22·5
r.m.s. bond length deviation (Å)	0·014	0·017	0·019	0·018	0·018
r.m.s. angular deviation (deg.)	2·8	3·3	3·5	3·4	3·8
r.m.s. dihedral deviation (deg.)	20·2	21·4	20·4	21·3	22·9
r.m.s. planar angle deviation (deg.)	1·5	1·6	1·5	1·8	2·0
Average temperature factor (all atoms) (Å^2)	29·0‡	24·4	25·1	34·5§	27·0§
Amino acid residues *included in the final* structure	25–76 and 88–184	25–76 and 88–180	25–76 and 88–180	25–76 and 88–180	25–76 and 88–180
Total number of protein non-hydrogen atoms	1166	1138	1138	1138	1138
Total number of water molecules	127	74	46	0	0
Total other atoms	7 phenan‖	0	2 Au	2 Hb	0.5 Pt¶

† Au reflections include Bijvoet pairs; anomalous scattering effects from the 2 Au atoms were included in the refinement.
‡ Includes 127 water molecules and phenanthroline.
§ Refined temperature factors as groups rather than as individual atoms.
‖ One molecule of 1,10-phenanthroline is shared equally between 2 receptor subunits and lies on the 2-fold relating these subunits. There are 14 non-hydrogen atoms in 1 molecule of 1,10-phenanthroline.
¶ One Pt atom is shared equally between 2 receptor subunits and lies on the 2-fold relating these subunits.

$$R_{\text{factor}} = 100 \times \sum_{hkl} \frac{|F_o(hkl) - F_c(hkl)|}{|F_o(hkl)|}.$$

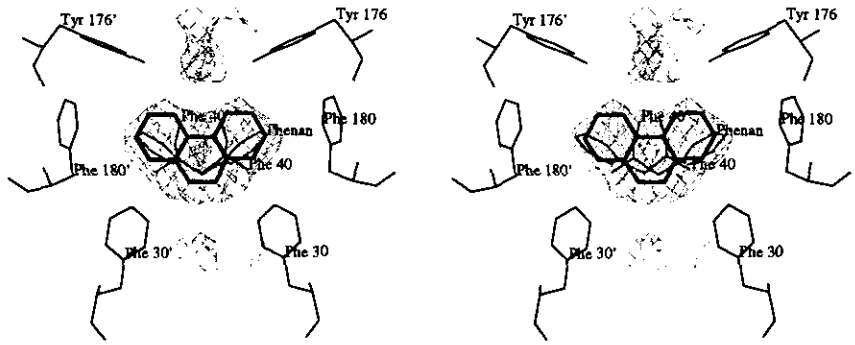

Figure 3. Stereo view of a difference Fourier contoured at 3σ illustrating the electron density corresponding to 1,10-phenanthroline buried at the interface of the 2 asparate receptor periplasmic domain subunits. Aromatic residues that form the phenanthroline binding pocket are labelled. The twofold axis of phenanthroline (a molecule with 2/m symmetry) is coincident with the crystallographic twofold axis relating one receptor subunit to the other.

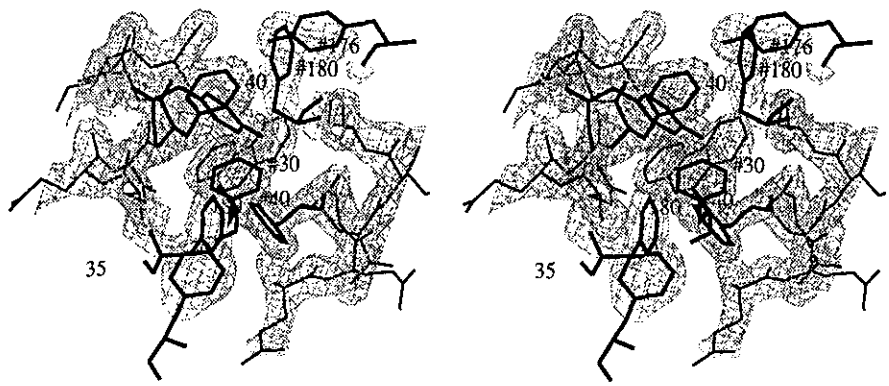

Figure 4. The solvent-flattened Au and Hg multiple isomorphous replacement with Au anomalous scattering electron density map illustrating the electron density associated with several aromatic side-chains in the putative aromatic ligand binding pocket. 1,10-Phenanthroline is indicated by light grey bonds.

R-factor of 18·8% for all 11,254 $F>2\sigma$ reflections between 6·0 and 2·2 Å resolution. The r.m.s. deviation from ideality for bond lengths is 0·014 Å and the r.m.s. deviation from ideality for bond angles is 2·8°. (These and other refinement statistics are summarized in Table 4.) A plot for the distribution of *R* factor values *versus* resolution (Luzzati, 1952) indicates that the expected error in the atomic co-ordinates for the currently refined structure is between 0·2 and 0·3 Å. The accuracy of the co-ordinates of the disordered regions such as the N and C termini and loop 1 is, of course, quite a bit lower. The integrity of the backbone geometry may be assessed with a Ramachandran plot (Ramachandran & Sassiekharan, 1968; Fig. 5); all residues except a glycine adopt standard backbone geometry.

The variation of the average main-chain temperature factor values over the amino acid sequence of the protein is shown in Figure 6. Disorder appears to be confined rather strictly to the N and C termini of the receptor fragment (as well as to the omitted loop 1); these regions have an average main-chain temperature factor greater than 30 Å^2. Interestingly, loops 2 and 3 appear to be rather rigid compared to loop 1. The electron density for the omitted loop 1 is extremely weak and ambiguous; therefore, the exact location and conformation of these residues are ill defined and thus are not included in the atomic model. Collecting diffraction data from a different crystal form or at lower temperatures may help to locate these residues more

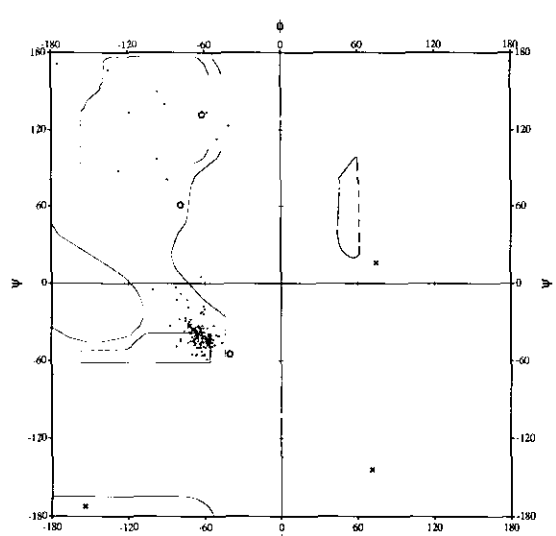

Figure 5. Ramachandran plot of the ϕ/ψ angles for the subunit of the periplasmic domain after refinement. The crosses are glycine residues and the pentagons are proline residues.

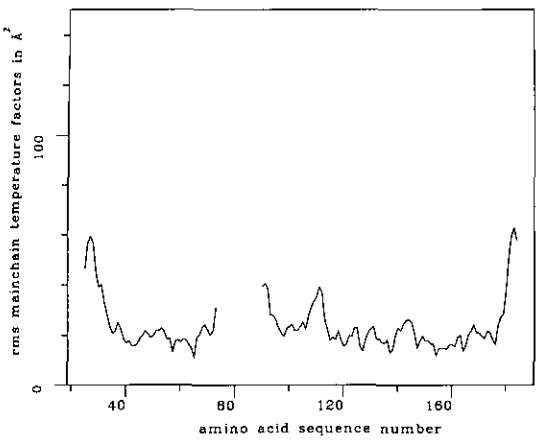

Figure 6. Plot of r.m.s. main-chain temperature factor *versus* amino acid residue number. Thermal disorder is confined primarily to loop 1 (residues 77 to 87; omitted from the refinement) as well as the N and C termini of the protein (residues 25 to 30 and 181 to 184).

accurately. However, it is quite possible that loop 1 is inherently flexible, and that such flexibility serves a biological function for the receptor.

The atomic model of the periplasmic domain subunit of the aspartate receptor crystallized in the absence of phenanthroline (residues 25 to 76 and 88 to 180) has an *R*-factor of 20·9%. (Additional refinement statistics for this and the metal ion structures are reported in Table 4.) The most significant differences between the two crystal structures were localized to the aromatic binding pocket region.

4. Discussion

(a) *Backbone structure of subunits: a four-α-helical bundle*

An overall view of the three-dimensional backbone structure of the ligand-binding domain of the aspartate receptor monomeric subunit is shown in Figure 1. Immediately apparent is the four-α-helical bundle motif first described by Argos *et al.* (1977). The first or N-terminal helix (helix 1) in our crystal structure of the ligand binding domain begins at serine 32. Helix 1 spans the length of the periplasmic domain to methionine 76, yielding a continuous 12-turn helix with 44 amino acid residues. A disordered loop (loop 1) of ten amino acid residues connects helix 1 to helix 2, which begins at lysine 86 and extends to asparagine 109, packing 18° from antiparallel upon helix 1. A second loop of seven residues (loop 2) then links helix 2 to helix 3. Helix 3 begins at methionine 116 and runs 18° from antiparallel to helix 2. Helix 3 finally gives rise to loop 3 at glycine 144. This third loop spans ten residues to threonine 154, but not before making a brief helical excursion between methionine 146 and glutamine 152. Finally, helix 4 begins at threonine 154 and runs 18° from antiparallel to helix 1, terminating at phenylalanine 180, thus completing the four-α-helical bundle motif of the aspartate receptor periplasmic domain. The overall structure of the aspartate-binding domain thus conforms to that predicted on the basis of biochemical data and sequence analysis (Moe & Koshland), but differs in detail.

The geometric properties of packed α-helices have been studied extensively by Chothia and others (Chothia *et al.*, 1977, 1981) who predicted, by fitting the ridges of side-chains from one helix into the grooves between side-chains of the other helix, that two antiparallel α-helices will pack most efficiently in two distinct ways. In one helix packing scheme, e.g. in four-helix bundle proteins, the crossing angle of adjacent helices is about 18° from antiparallel to minimize steric interference from the helix side-chains, and in the other helix packing scheme (as in hemoglobin) the crossing angle is about 50° from antiparallel. Our structure indeed conforms to the four-helix bundle packing prediction. Each residue at the interface between antiparallel helices can make contact with two residues contributed by the neighboring helix. The most pronounced of these side-chain interactions between the helices within the four-helix bundle are listed in Table 5. The geometry and common topology of four-α-helical bundle proteins subsequently have been analyzed (Cohen & Parry, 1990) and the sequentially connected left-twisted bundles of haemerythrin, apoferritin, tobacco mosaic virus coat protein, cytochrome *b*562 and cytochrome *c'* as well as a genetically engineered four-α-helical bundle all display similar gross geometry and identical connectivity (Weber & Salemme, 1980).

(b) *Aspartate binding sites: "half-pocket" per subunit*

A series of site-directed cysteine crosslinking experiments recently has established unambiguously that the intact aspartate receptor exists as a dimer both in the absence and the presence of bound aspartate (Milligan & Koshland, 1988). These experiments also clearly demonstrate that ligand binding inhibits the rapid exchange of subunits between dimeric receptors. Examination of a ribbon model generated from the crystal structure of the intimately entwined crosslinked dimer of the aspartate-binding domain (Figs 2 and 4) as well as the corresponding C^{α} plot of the dimer (Fig. 7) helps to explain the latter observation. Threonine at position 154 (Lee & Imae, 1990) as well as three arginine residues, at positions 64, 69 and 73 (Wolff & Parkinson, 1988; Mowbray & Koshland, 1990), have been implicated previously in aspartate binding. Arginine 64 and threonine 154 of one subunit conspire with arginine residues 69 and 73 of the other subunit to form a charged pocket that binds a single molecule of aspartate, as shown schematically in Figure 8 (Milburn *et al.*, 1991). Both receptor halves are involved in binding each aspartate ligand, serving to lock the two monomers together and thereby inhibiting subunit exchange.

Only one aspartate binds to the receptor subunit

Table 5
Atomic contacts within the 4 α-helix bundle subunit

Helix 1		Helix 2		Distance (Å)
Gln49	O	Phe107	$C^{\delta1}$	3·60
Glu52	$O^{\varepsilon2}$	His103	$C^{\delta2}$	2·95
Glu52	$O^{\varepsilon2}$	Asn106	$N^{\delta2}$	2·96
Glu52	C^{β}	Phe107	C^{β}	3·82
Leu53	$C^{\delta2}$	Phe107	$C^{\delta2}$	3·57
Ser55	O^{γ}	His103	$N^{\varepsilon2}$	3·65
Thr56	C^{β}	Ala100	O	3·36
Thr56	C^{β}	His103	C^{β}	3·98
Thr56	$C^{\gamma2}$	Tyr104	C^{α}	3·91
Leu59	O	Thr96	$O^{\gamma1}$	3·94
Leu59	$C^{\delta2}$	Gln99	C^{β}	3·89
Leu59	C^{β}	Ala100	C^{β}	3·78
Leu59	$C^{\delta2}$	His103	$N^{\delta1}$	3·54
Met60	C^{γ}	Ala100	C^{β}	3·71
Gln62	O	Thr96	$O^{\gamma1}$	4·39
Thr63	$C^{\gamma2}$	Ala93	O	3·76
Thr63	$O^{\gamma1}$	Thr96	$O^{\gamma1}$	2·94
Thr63	$C^{\gamma2}$	Leu97	C^{γ}	3·89
Asn66	O	Leu89	O	3·68
Asn66	$O^{\delta1}$	Asn92	$N^{\delta2}$	3·94
Asn66	$N^{\delta2}$	Thr96	$O^{\delta1}$	4·16
Leu67	$C^{\delta1}$	Leu90	$C^{\delta2}$	3·77
Leu67	$C^{\delta1}$	Ala93	C^{β}	3·37
Arg69	$N^{\eta1}$	Leu89	$C^{\delta1}$	2·97
Arg69	$N^{\eta1}$	Asn92	$O^{\delta1}$	4·66
Ser70	O^{γ}	Leu89	C^{β}	3·06
Ser70	O^{γ}	Leu90	N	3·56
Arg73	C^{δ}	Leu89	$C^{\delta2}$	3·59

Helix 1		Helix 4		Distance (Å)
His35	$N^{\varepsilon2}$	Thr179	O	3·69
Gly39	C^{α}	Thr179	C^{β}	3·64
Ile42	$C^{\gamma2}$	Leu175	$C^{\delta1}$	3·88
Ile42	$C^{\delta1}$	Thr179	$C^{\gamma2}$	4·12
Ser43	O^{γ}	Tyr176	$C^{\varepsilon1}$	2·94
Leu46	$C^{\delta2}$	Leu175	$C^{\delta1}$	3·81
Gln49	$N^{\varepsilon2}$	Tyr168	O^{η}	2·72
Gln50	$N^{\varepsilon2}$	Ser172	O^{γ}	3·98
Gln50	$O^{\varepsilon1}$	Tyr168	$C^{\delta2}$	4·10
Leu53	$C^{\delta2}$	Leu165	$C^{\delta2}$	4·22
Leu53	$C^{\delta1}$	Tyr168	$C^{\delta2}$	3·59
Trp57	$C^{\eta2}$	Gln158	C^{γ}	3·70
Trp57	$C^{\varepsilon3}$	Leu161	$C^{\varepsilon2}$	3·78
Trp57	$C^{\eta2}$	Gly162	C^{α}	3·65
Trp57	$C^{\delta1}$	Leu165	$C^{\delta1}$	3·59
Met60	S^{δ}	Leu161	$C^{\delta2}$	4·07
Leu61	$C^{\delta1}$	Gln158	C^{δ}	3·81
Arg64	$N^{\eta1}$	Thr154	$O^{\delta1}$	3·81
Arg64	$N^{\eta2}$	Gln155	$O^{\varepsilon1}$	2·60
Arg64	$N^{\eta2}$	Gln158	$O^{\varepsilon1}$	2·91

Helix 2		Helix 3		Distance (Å)
Lys86	N^{ζ}	Asp142	$O^{\delta2}$	3·33
Leu90	$C^{\delta2}$	Ile138	$C^{\gamma2}$	4·50
Leu90	$C^{\delta2}$	Leu142	C^{β}	4·03
Leu90	$C^{\delta1}$	Asp142	N	3·60
Ala93	C^{β}	Ile138	$C^{\delta1}$	4·15
Lys94	C^{ε}	Ile138	$C^{\gamma2}$	3·70
Lys94	N^{ζ}	Asp142	$O^{\delta2}$	2·97
Leu97	$C^{\delta2}$	Gln131	$O^{\varepsilon1}$	3·69
Leu97	C^{γ}	Leu134	C^{β}	4·09
Leu97	$C^{\delta1}$	Ala135	C^{α}	3·79
Ala101	C^{α}	Tyr127	O^{η}	3·11
Tyr104	O^{η}	Asp124	$O^{\delta2}$	2·92
Tyr104	C^{γ}	Tyr127	C^{ζ}	3·70
Phe107	C^{ζ}	Ser120	O^{γ}	4·26
Lys108	N^{ζ}	Asp124	$O^{\delta2}$	2·80
Lys108	N^{ζ}	Gln128	$O^{\varepsilon1}$	3·64

Table 5 (*continued*)

Helix 2		Helix 4		Distance (Å)
Phe107	C^{ζ}	Tyr168	$C^{\varepsilon1}$	3·81

Helix 1		Helix 3		Distance (Å)
Leu46	$C^{\delta1}$	Met116	C^{γ}	4·29
Leu53	$C^{\delta2}$	Val123	$C^{\gamma1}$	3·93
Thr56	$O^{\gamma1}$	Tyr127	$C^{\varepsilon1}$	3·57
Thr56	$O^{\gamma1}$	Tyr127	$O^{\eta1}$	4·97
Try57	$C^{\zeta3}$	Tyr130	$C^{\zeta1}$	4·31
Met60	S^{δ}	Tyr127	$C^{\varepsilon1}$	3·77
Met60	C^{ε}	Tyr130	$C^{\delta1}$	3·43
Met60	C^{ε}	Gln131	C^{α}	3·59
Met60	C^{β}	Leu134	$C^{\delta2}$	3·91
Thr63	C^{β}	Leu134	C^{γ}	4·20
Arg64	$N^{\eta2}$	Tyr130	O^{η}	3·16
Arg64	$C^{\delta2}$	Leu137	C^{β}	4·08
Leu67	$C^{\delta1}$	Ile138	$C^{\delta2}$	3·83
Met74	C^{ε}	Leu141	C^{β}	3·99

Helix 3		Helix 4		Distance (Å)
Met116	S^{δ}	Tyr168	C^{ζ}	4·34
Met116	C^{ε}	Val171	$C^{\gamma1}$	3·53
Met116	S^{δ}	Ser172	O^{γ}	3·73
Met116	C^{ε}	Leu175	$C^{\delta1}$	3·66
Ala119	C^{β}	Asn167	$O^{\delta1}$	4·11
Ala119	C^{β}	Tyr168	$C^{\delta1}$	3·99
Ser120	O^{γ}	Tyr168	$C^{\varepsilon1}$	3·17
Asn122	$N^{\delta2}$	Asn167	$O^{\delta1}$	4·20
Val123	$C^{\gamma1}$	Leu165	$C^{\delta2}$	4·03
Val123	$C^{\gamma2}$	Tyr168	C^{β}	3·95
Lys126	C^{γ}	Ala160	C	3·70
Lys126	C^{β}	Leu161	C^{α}	3·65
Tyr127	N	Leu161	$C^{\delta1}$	3·99
Arg129	O	Met157	S^{δ}	4·00
Tyr130	$C^{\varepsilon2}$	Thr154	$C^{\gamma2}$	4·03
Tyr130	$C^{\delta2}$	Met157	C	3·90
Tyr130	O^{η}	Gln158	$O^{\varepsilon1}$	2·80
Tyr130	$C^{\varepsilon2}$	Leu161	$C^{\delta2}$	3·69
Leu137	$C^{\delta1}$	Thr154	$C^{\gamma2}$	3·86

dimer in the crystal structure reported previously (Milburn *et al.*, 1991), suggesting an asymmetry in the two potential aspartate binding sites. Negative cooperativity in aspartate binding in both the periplasmic domain and in the intact aspartate receptor subsequently has been observed (H.-P. Biemann & D. E. Koshland, unpublished results). Side-chain torsion angle conformational changes of arginine 64 in the unoccupied binding site relative to that in the refined crystal structures of the ligand-binding domain in the absence of aspartate may also be observed (Scott, 1992), indicating that binding of one aspartate molecule to the receptor inhibits binding of a second by altering the unoccupied binding site. No difference between the two unoccupied aspartate sites in the structures considered here is observed, because the two sites are related by exact twofold crystal symmetry.

(c) *The subunit dimer interface*

The dimer interface is comprised almost exclusively of interactions between helix 1 of one subunit and the crystallographic twofold related helix 1′ of

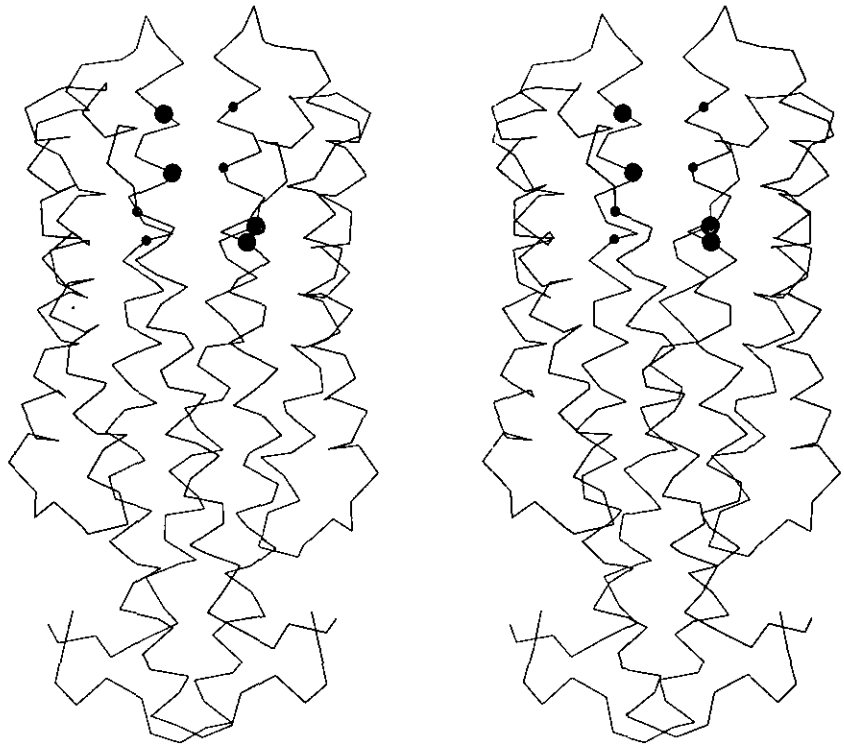

Figure 7. The C^{α} backbone structure (Kraulis, 1991) of the functionally active dimer of periplasmic domains of the aspartate receptor. Arginine residues 64, 69′ and 73′, and threonine 154 form one aspartate binding pocket and are shown as large black and gray circles, respectively. Arginine residues 64′, 69 and 73, and threonine 154′, shown likewise as small black and grey circles, form the other (unoccupied) aspartate binding pocket (after Milburn *et al.*, 1991).

the other subunit; virtually all of the surface area of the receptor subunit that is rendered solvent-inaccessible by dimerization of the periplasmic domains is comprised of helix 1 side-chains, as illustrated in Figure 9. Helix 1 and helix 1′ pack approximately 20° askew from parallel (see Fig. 10) in a manner similar to that first predicted by Crick (1953) in his analysis of the knobs-into-holes packing scheme of parallel α-helical coiled-coils. O'Shea *et al.* (1991) have observed parallel coiled-coil packing at the dimer interface of α-helical peptide fragments corresponding to the yeast transcriptional activator GCN4 "leucine zipper." The dimerization of GCN4 α-helices is mediated by continuous hydrophobic contacts between leucine residues and results in a left-handed superhelical coiling of the parallel α-helices of approximately 90° over the length of the 31-residue helices, as well as a helix crossing angle of approximately 18°. Although helix 1 and helix 1′ form an analogous (albeit imperfect) parallel coiled-coil at the aspartate receptor subunit interface, there are several important differences between the two structures. In the aspartate receptor periplasmic domain, the helical contacts are not contiguous, and electrostatic and hydrogen-bonding interactions as well as hydrophobic interactions mediate the helix 1-helix 1′ contacts. The most important of these contacts are listed in

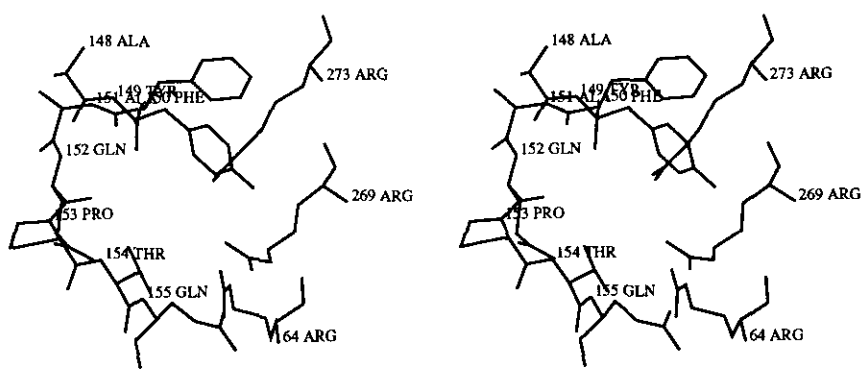

Figure 8. A stereo diagram of the aspartate binding site. Arginine 64, threonine 154 and tyrosine 149 of one subunit and arginine 269 and 273 of the other subunit compose the aspartate binding site.

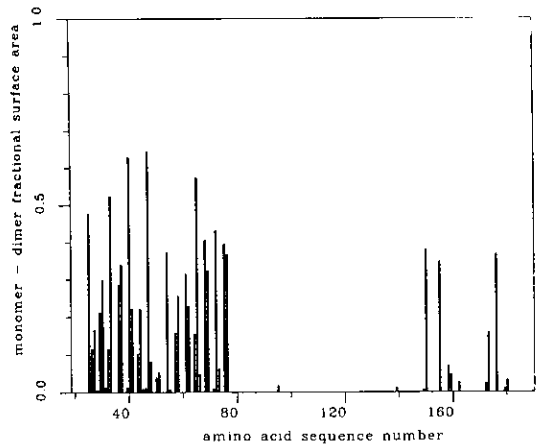

Figure 9. Histogram depicting the results of subtracting the solvent-accessible surface area (calculated using the method of Lee & Richards (1971) as implemented in XPLOR 2.1 (Brünger, 1990) using a probe of radius 1·6 Å) of the dimer (illustrated in Fig. 2) from the aspartate receptor ligand-binding domian subunit (illustrated in Fig. 1), revealing that virtually the entire dimer interface is composed of interactions between the N-terminal helices of each subunit, i.e. helix 1 and helix 1′. A few contacts between helix 1 and helix 4′ also occur; however, helix 4 and helix 4′ do not contact one another. These interactions are summarized in Table 6.

Table 6
Atomic contacts at the subunit dimer interface

Helix 1		Helix 1′		Distance (Å)
Ser32	C	Leu33′	C^{γ}	3·66
Leu33	$C^{\delta 1}$	Ser32′	C^{α}	4·17
Leu33	C^{γ}	Leu33′	C^{α}	4·09
Leu33	$C^{\delta 2}$	Cys36′	C^{β}	3·90
Cys36	S^{δ}	Cys36′	S^{δ}	2·29
Cys36	S^{δ}	Gln37′	N	3·78
Ser43	$C^{\delta 1}$	Arg47′	$N^{\eta 2}$	3·12
Thr54	O^{γ}	Thr54′	O^{γ}	3·44
Trp57	$N^{\varepsilon 1}$	Asp58′	$O^{\delta 1}$	3·06
Trp57	$N^{\varepsilon 1}$	Asp58′	$O^{\delta 2}$	3·71
Trp57	$N^{\varepsilon 1}$	Gln62′	$N^{\varepsilon 2}$	3·06
Asp58	$O^{\delta 1}$	Leu61′	$C^{\delta 2}$	3·86
Leu61	$C^{\delta 1}$	Leu61′	$C^{\delta 2}$	4·31
Leu61	$C^{\delta 2}$	Gln62′	C^{δ}	4·40
Leu61	C^{γ}	Ile65′	$C^{\delta 1}$	3·68
Arg64	C^{γ}	Ile65′	$C^{\delta 1}$	3·88
Arg64	$N^{\eta 1}$	Arg69′	C^{δ}	3·34
Arg64	$N^{\eta 1}$	Arg69′	$N^{\eta 2}$	4·51
Ile65	$C^{\delta 1}$	Ile65′	$C^{\delta 1}$	3·75
Ser68	O^{γ}	Ser68′	O^{γ}	3·56
Ala72	O	Met75′	S^{δ}	4·65
Met75	S^{δ}	Met75′	S^{δ}	5·43
Met75	C^{ε}	Met76′	C^{γ}	3·64
Helix 1		**Helix 4′**		**Distance (Å)**
Phe40	$C^{\varepsilon 2}$	Tyr176′	$O^{\eta 2}$	3·75
Phe40	$C^{\varepsilon 2}$	Phe180′	$C^{\delta 1}$	3·40
Ser43	O	Tyr176′	O^{η}	4·86
Asn44	$N^{\delta 2}$	Tyr176′	O^{η}	2·86
Asn44	$N^{\delta 2}$	Phe180′	$C^{\varepsilon 1}$	4·59
Arg47	$N^{\eta 2}$	Glu173′	$O^{\varepsilon 1}$	3·17
Arg47	$N^{\eta 2}$	Tyr176′	$C^{\delta 2}$	3·43
Ile65	$C^{\delta 1}$	Gln155′	$O^{\varepsilon 1}$	3·51
Asn66	$O^{\delta 1}$	Gln155′	$N^{\varepsilon 2}$	4·58
Arg69	$N^{\eta 2}$	Gln 155′	$O^{\varepsilon 1}$	3·51

There is no contact between helix 4 and helix 4′.
The monomers are related by crystallographic 2-fold symmetry. Symmetry-related contacts are therefore not listed.

Table 6. Local distortions in the helices also result in imperfect packing, notably near serine 68 where the two C^{β} carbon atoms approach closely, and in the region between serine 43 and threonine 54, where the helices bow out and few contacts between the side-chains occur. The helix crossing angle is approximately 20° from parallel, similar to the optimal packing angle of two parallel α-helices predicted by Crick (1953). Helix 1 and helix 1′ also bend toward one another near the N terminus as may be seen most clearly in Figure 2; presumably this is a distortion caused by the presence of the cysteine 36 cross-link.

(d) *The aromatic binding pocket and its possible biological significance*

The density assigned to the aromatic ligand phenanthroline is located on the crystallographic twofold axis and is thus shared equally by both subunits of the dimer (Figs 3 and 4). The plane containing the phenanthroline molecule is perpendicular to the plane tangent to the interface of the two subunits of the dimer that contains the crystallographic twofold axis. The aromatic pocket in which phenanthroline binds is located near the transmembrane region of the receptor and is composed of Phe30, Phe40 Phe180 and Tyr176, as well as their four symmetry pairs. These eight aromatic side-chains line the binding pocket and form a tightly packed network of hydrophobic interactions with the aromatic phenanthroline ligand, as shown in Figure 11. In the absence of phenanthroline, these aromatic side-chains, notably Phe40 and Tyr176, rearrange to a different conformation such that they are able to interact with one another and partially seal the aromatic binding pocket.

Phenanthroline, of course, is not a naturally occurring aromatic ligand in the environment of *S. typhimurium* and *E. coli*. Although the specific binding of phenanthroline to the aspartate receptor may be merely an artifact of the crystallization experiment, several lines of reasoning suggest that the aromatic binding site may nonetheless be important biologically for sensing small aromatic compounds. Phenol is known to induce chemotaxis in *S. typhimurium* and *E. coli* (Lederberg, 1956; Tso & Adler, 1974), and recently has been demonstrated to bind to the aspartate receptor, eliciting an attractant response (Imae *et al.*, 1987). We do not have direct evidence to suggest that phenol (or a related aromatic metabolite) is the natural ligand for this aromatic binding pocket, but the phenanthroline binding site is an obvious candidate for such a site. (This hypothesis can be tested using phenanthroline

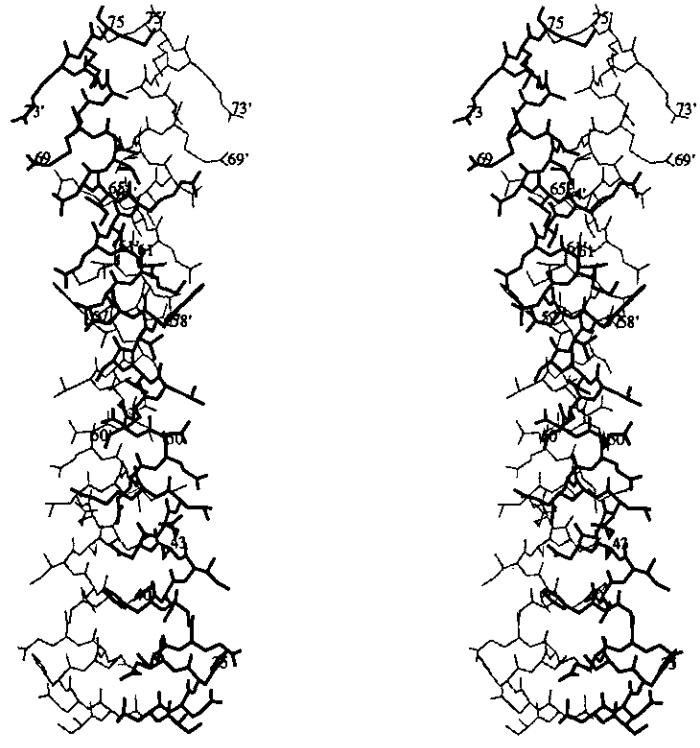

(a)

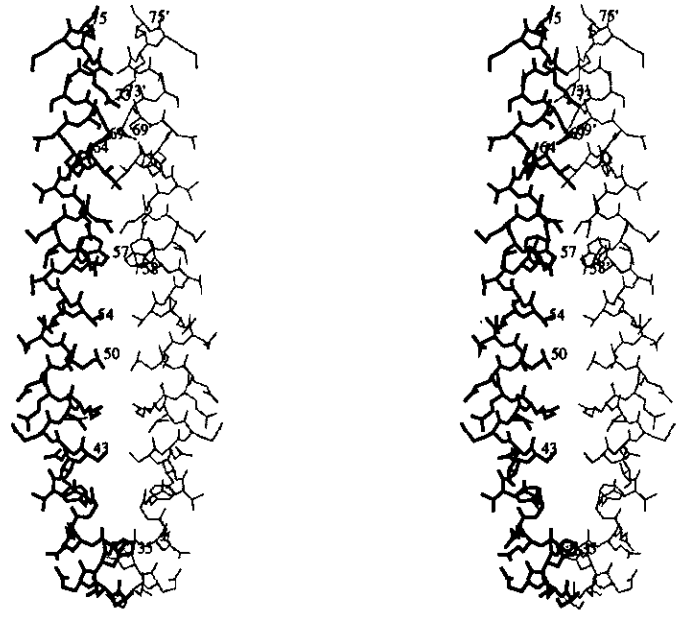

(b)

Figure 10. (a) Helix 1 and helix 1′ are shown to cross at an angle of approx. 20° in this stereo view. The accompanying Table 6 lists the primary side-chain interactions responsible for mediating the dimer interface contacts in these helices. (b) A 90° rotation of (a).

in a standard chemotaxis swarm-assay experiment and by crystallizing the receptor domain in the presence of phenol.) Similar to the aspartate binding site, this putative aromatic chemoeffector binding site is located at the subunit interface.

(e) *Possible biological significance of metal binding sites*

In addition to aspartate and phenol, the aspartate receptor has the ability to detect and respond to metal ions encountered by bacteria. Unchelated

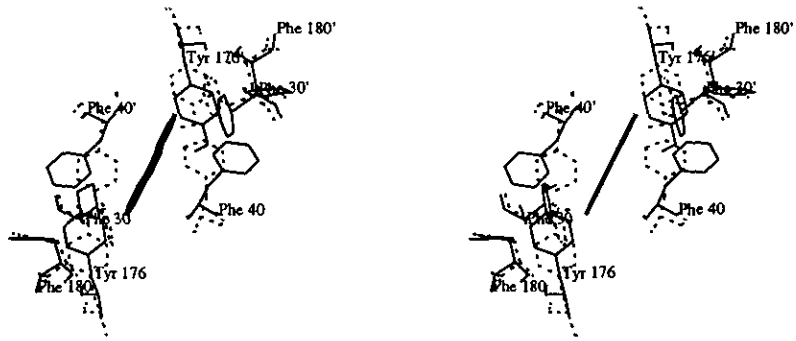

Figure 11. Stereo diagram, viewed along the plane of 1,10-phenanthroline, illustrating the extensive aromatic interactions taking place with 1,10-phenanthroline in the putative aromatic ligand pocket. Aromatic side-chains which rearrange conformation in the absence of phenanthroline are indicated with broken bonds.

Co^{2+} and Ni^{2+} have been shown to act as chemotaxis repellents in *E. coli* (mediated by the aspartate receptor: Tso & Adler, 1974), but not in *S. typhimurium* (Ingolia & Koshland, 1979; Macnab, 1987). However, in *S. typhimurium*, both ions act as weak chemoattractants when complexed with citrate (Ingolia & Koshland, 1979; Macnab, 1987). There is no clear evidence for attraction to other inorganic compounds in either species (Macnab, 1987), and inorganic repellent effects have been established only for Co^{2+}, Ni^{2+}, S^{2-} and mercaptans in *E. coli* (Tso & Adler, 1974; Macnab, 1987). It is, however, worth examining the binding sites for the heavy-metal complex ion derivative crystals that were prepared for isomorphous replacement phase calculations to see if any of these might reveal potential biologically relevant metal-binding sites.

The binding sites for Au(I), Hg(II) and Pt(IV) on the aspartate receptor periplasmic domain are illustrated together in the context of a ribbon diagram (Fig. 12). The major Au(I) site lies close to the subunit interface of the receptor dimer, where an Au(I) atom appears to be bound to the $O^{\varepsilon 1}$ and $N^{\varepsilon 2}$ of glutamine 50 in a tetrahedral configuration. A second Au(I) site is located at asparagine 159, where Au(I) is bound linearly to the carbonyl oxygen atom. Aside from a slight movement of the glutamine 50 side-chain, Au(I) binding to the aspartate receptor appears to cause little structural perturbation. The two Hg(II) sites are at the N terminus and tryptophan 57. In both cases, Hg(II) binds with a tetrahedral geometry. Again the structural perturbations appear minimal.

A more interesting situation may exist in the case of the Pt-bound receptor structure, which was not used for MIR phase calculaton. Six methionine residues (74, 75, 76 and their symmetry mates) reside in close spatial proximity at the C-terminal ends of helix 1 and helix 1′. These six methionine residues are conserved in the *E. coli* aspartate receptor and four methionine residues (75, 76 and their symmetry mates) are conserved in the more distantly related *E. coli* Tsr or serine chemotaxis receptor. This unusual conserved structural arrangement suggests that the receptor may employ this methionine-rich pocket in some sensory-related function. Indeed, the sole Pt(IV) site lies directly on the crystallographic twofold axis, where the Pt atom is shared symmetrically between methionine 75 of one subunit and methionine 75′ of the symmetry-related subunit (Fig. 12). Pt(IV) maintains the octahedral geometry of the $K_2Pt(SCN)_6$ complex, but the carbonyl oxygen atoms of methionine 75 and methionine 75′ replace one pair of twofold symmetry-related thiocyanate groups, and the S^{δ} side-chain atoms of methionine 75 and methionine 75′ replace a second such pair; the final pair appear to remain in place.

Pt(IV) binding appears to have a more pronounced effect upon the conformation of the receptor ligand-binding domain, especially in the neighborhood of residues 72 to 75 of helix 1 and

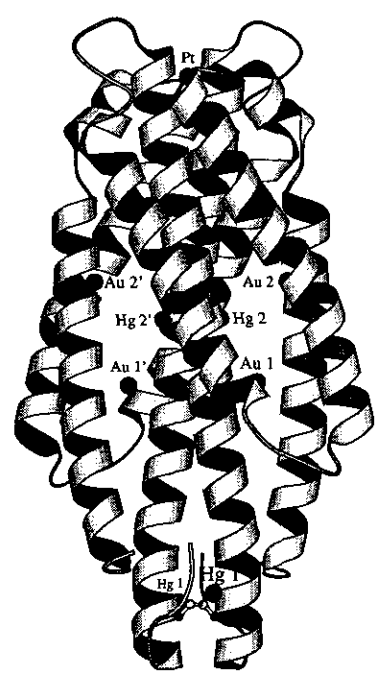

Figure 12. Heavy-atom derivative binding sites. Ribbon diagram (Kraulis, 1991) illustrating the locations of the 2 Au(I) binding sites, the 2 Hg(II) binding sites and the Pt(IV) binding site.

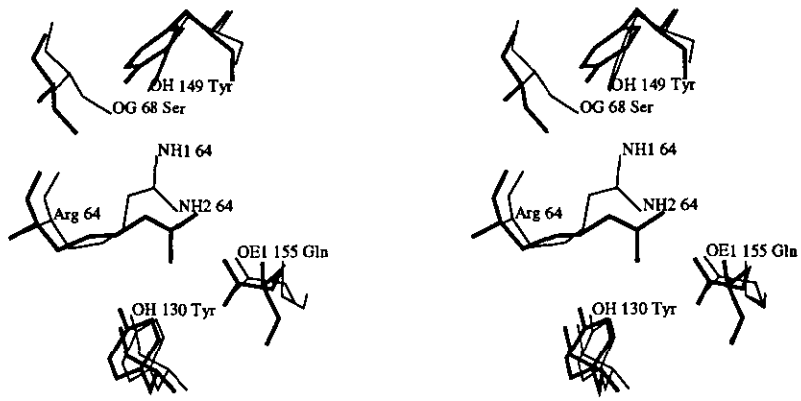

Figure 13. Stereo view of the torsion angle conformational changes in arginine 64 as they take place in the 2 crystal structures. The native structure is represented with dark lines, and the Pt bound structure is represented with lighter lines. In the native structure, the amino hydrogen atoms of arginine 64 form hydrogen bonds with the tyrosine 130 hydroxyl oxygen atom (3·1 Å) and glutamine 155 carbonyl oxygen atom (2·6 Å). In the Pt-bound structure, arginine 64 *rearranges conformation to form hydrogen bonds to the tyrosine 149 hydroxyl oxygen atom (2·75 Å) and serine 68* hydroxyl oxygen atom (2·95 Å).

residues 152 to 154 of helix 4. The side-chain of arginine 64 in particular (which is involved in aspartate binding and is found to change conformation in the unoccupied ligand-binding pocket as described in section (c), above), rearranges its amine-hydrogen-bonding pattern from interactions with glutamine 155 $O^{\varepsilon 1}$ and tyrosine 130 O^{η} in the two native structures to interactions with serine 68 O^{γ} and *tyrosine 149* O^{η} *in the Pt derivative structure* (Fig. 13).

Interestingly, an investigation of the extent of amino acid binding-site conservation between the otherwise dissimilar tryptophan repressor and the aspartate receptor suggests that a similar rearrangement of the hydrogen-bonding network within the amino acid binding site of both proteins may play a crucial role in mediating the transmembrane signalling event (Lynch & Koshland, 1992).

The Pt(IV) complex ion binds to the receptor subunit interface in such a way that this ligand is shared between the two subunits of the receptor in a manner analogous to that of the ligands aspartate and phenanthroline. Moreover, maltose-binding protein (an attractant) has been suggested to interact with loop 1 and adjacent residues on helix 1 of the *E. coli* aspartate receptor, including methionine 75 (Kossmann *et al.*, 1988; Gardina *et al.*, 1992.). *A simulated "docking" of the maltose-binding protein to this methionine-rich region of the E. coli* receptor (Stoddard & Koshland, 1992) provides support for the hypothesis that this methionine-rich pocket region is relevant to the mechanism of transmembrane signalling.

These observations considered together strongly suggest that Pt(IV) may be binding to a biologically relevant site on the protein. Pt(IV) binding to the methionine-rich pocket of the aspartate receptor may thus mimic the effect of known metal chemorepellants (or perhaps other chemoattractants) by inducing side-chain torsion-angle conformational changes in the aspartate-binding site, which are in turn responsible for initiating the transmembrane-signalling event (in a manner similar to that described for conformational changes in insulin as suggested by Chothia *et al.*, 1983).

(f) *Understanding chemotaxis receptor structure-function relationships based upon the aspartate-binding domain crystal structure*

The crystal structure of the ligand-binding domain of the aspartate receptor enables us to make some fairly conservative structural predictions. Lynch & Koshland (1991) have shown that crosslinking residues 18 and 18′ produces an active signalling protein. Since it was already known that the 36–36′ crosslinking also produces an active signalling protein, this fits an uninterrupted α-helix extending from residue 36 to residue 18 and presumably at least to the cytoplasmic side of the membrane. Such a structure was indeed postulated *as an extension of the crystal structure (Milburn et al.*, 1991). The second prediction is that other members of the bacterial chemotaxis transmembrane receptor family have periplasmic domain three-dimensional structures similar to that of the *S. typhimurium* aspartate receptor. These predictions not only are supported by mutagenisis experiments but also help to explain the results of the experiments, as will be described below.

(i) *The* Salmonella typhimurium *aspartate receptor: modelling the membrane spanning regions*

To understand aspartate receptor-mediated transmembrane signalling, it will be helpful to model the structure of the intact transmembrane receptor protein as it might appear in the membrane based upon the crystal structure of the aspartate-binding domain. The membrane-spanning regions of the protein have been modelled in such a way that they are consistent with the known structures as

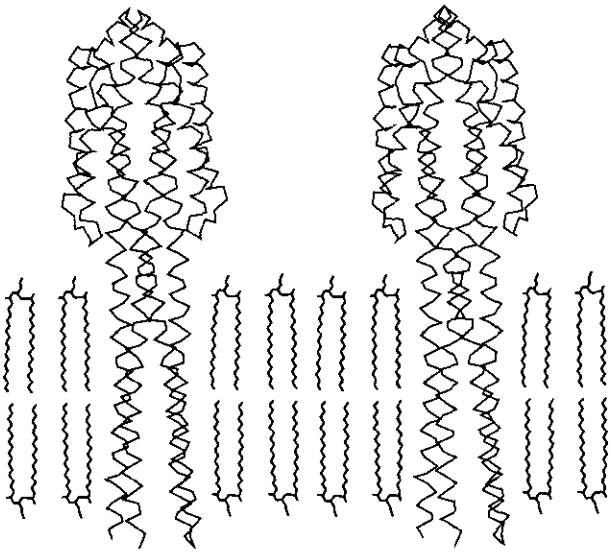

Figure 14. Diagram of the aspartate receptor dimer with the modelled transmembrane regions consisting of uninterrupted continuations of helices 1 and 4 from each 4-α-helix bundle subunit. The primary interactions between the helices in the membrane are believed to be restricted to those between helix 1 and helix 1′.

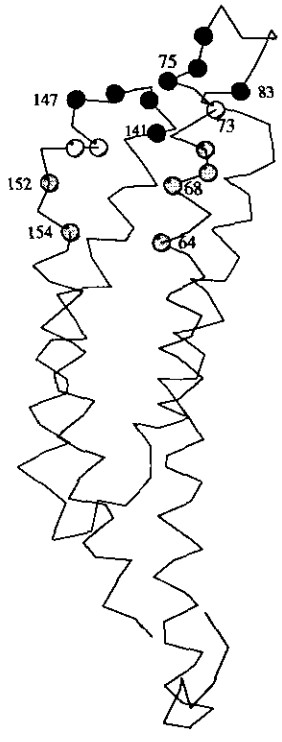

Figure 15. Schematic representation of amino acid mutations that impair *E. coli* aspartate receptor signalling as displayed on a C^{α} backbone structure (Kraulis, 1991) of one subunit. The Asp^- phenotype mutations (64, 68, 69, 70, 152 and 154) correspond to the gray circles and are proximal to the aspartate binding site. The Mal^- phenotype mutations (75, 76, 77, 83, 141, 143, 145 and 147) correspond to the black cirlces and are located on or near loops 1 and 3. The Asp^- Mal^- double phenotype mutations (73, 149 and 150) are represented as white circles.

well as with the constraints imposed by the membrane (Milburn *et al.*, 1991). The putative membrane-spanning regions of the protein sequence (residues 7 to 30 and 189 to 212) are quite hydrophobic in character (Russo & Koshland, 1983) and these regions are predicted to form two α-helices (Falke *et al.*, 1988; Lynch & Koshland, 1991), which continue uninterrupted from the N and C-terminal helices of the aspartate-binding domain crystal structure. The placement and orientation of the extended helices were restricted to coincide with those of the crystal structure, and the energy optimization incorporated protein dimer interactions. The resulting model of the aspartate-binding domain dimer with attached membrane-spanning helices is depicted in Figure 14.

The two α-helical membrane-spanning regions of the receptor match up exactly to the starting and ending amino acid residues based on hydrophobicity predictions, thus allowing favorable interaction between the two transmembrane segments. There are several side-chain interactions between the N-terminal membrane-spanning regions of the two monomers and these are essentially the only interactions between the two receptor halves in this region. The C-terminal helix membrane-spanning region forms a very loose contact with the N-terminal helix within the subunit. These interactions and the relative placement of the membrane-spanning regions are consistent with the results of recent cysteine cross-linking studies (Lynch & Koshland, 1991; Pakula & Simon, 1992) and may well be important in dimer formation and signal transduction in the intact aspartate receptor.

(ii) *The* E. coli *aspartate receptor*

The *E. coli* aspartate receptor (unlike its *S. typhimurium* cousin) binds to maltose-binding protein when this latter soluble periplasmic protein is complexed with maltose or a maltodextrin (Koiwai & Hayashi, 1979; Richarme, 1982; Manson *et al.*, 1985). The response of the *E. coli* aspartate receptor to maltose and aspartate has been shown to be independent and additive (Mowbray & Koshland, 1987). A number of mutations that interfere with aspartate chemotaxis (Asp^-) or maltose chemotaxis (Mal^-) have been identified. Mutations affecting residues 64 to 73 or 149 to 154 have an (Asp^-) phenotype, and mutations affecting residues 73 to 83 or 141 to 150 have a (Mal^-) phenotype (Fig. 15). Mutations in residues 73, 149 and 150 may also have an (Asp^- Mal^-) phenotype (Gardina *et al.*, 1992).

Assuming the three-dimensional structure of the *E. coli* aspartate receptor is essentially the same as that of *S. typhimurium*, the basis of these mutant phenotypes immediately becomes apparent. Residues 64 to 73 and 149 to 154 are involved in forming the aspartate-binding pocket, so mutations involving these sites will have the Asp^- phenotype.

Residues 73 to 83 constitute the last two amino acid residues of helix 1 and most of the flexible loop 1 that connects helix 1 to helix 2. Residues 141 to 150 reside in loop 3, which connects helix 3 to helix 4 (Fig. 15). Therefore, it appears quite likely that loops 1 and 3 (along with residues 73 to 75 of helix 1) form the binding site for maltose-binding protein. These results are consistent with the simulated docking of maltose-binding protein to the *E. coli* aspartate receptor periplasmic domain, which was based upon the assumption that the *E. coli* and *S. typhimurium* aspartate receptor periplasmic domain three-dimensional structures were essentially the same (Stoddard & Koshland, 1992).

(iii) *The* E. coli *ribose and galactose-binding proteins receptor (Trg receptor)*

The Trg receptor binds to either of two periplasmic binding proteins in a manner presumably similar to the way in which the *E. coli* aspartate receptor binds to the maltose-binding protein (Adler *et al.*, 1973; Strange & Koshland, 1976; Harayama *et al.*, 1983; Bollinger *et al.*, 1984). Therefore, by modelling the Trg receptor periplasmic domain based upon the aspartate receptor crystal structure, we should be able to understand how the periplasmic ribose-binding protein complexed to ribose and to galactose-binding protein complexed to galactose will bind Trg receptor.

Yaghmai & Hazelbauer (1992) have constructed mutations within residues 69 to 88 in the Trg receptor sequence (which correspond to residues 59 to 78 in the aspartate receptor structure due to a different sequence numbering scheme). They discovered two distinct mutant phenotypes, both of which affect receptor signalling. The first phenotype causes the receptor to signal constitutively in the absence of a bound ligand; these mutations essentially turn the receptor signal on. (These mutations appear in residues 71 to 79 in the Trg receptor and correspond to residues 61 to 69 in the aspartate receptor structure.) The second phenotype consists of mutations that reduce or eliminate responses to stimulation by sugar attractants; they essentially turn the receptor signal off. (These mutations are in residues 79 to 86 in the Trg receptor, which correspond to residues 69 to 76 in the aspartate receptor structure.) Mutations at residue 79 result in both phenotypes.

A model of the dimeric periplasmic domain of the Trg receptor based on that of the aspartate receptor (which takes into account the different sequence numbering schemes) places the region corresponding to the first or on phenotype (residues 71 to 79) deeply within the helix 1 – helix 1′ subunit interface of the receptor dimer. Amino acid side-chains in this region are intimately involved in hydrophobic contacts at the dimer interface. The region corresponding to the second or off phenotype (residues 79 to 86) are located at the more solvent-accessible C-terminal end of helix 1 (Fig. 16). We calculated the solvent accessibility of residues 71 to 86 using the method of Lee & Richards (1971) to estimate the degree of exposure of these amino acid residues. The transition between buried residues and exposed residues occurs sharply at residue 79, which is at the interface between the two regions of mutations.

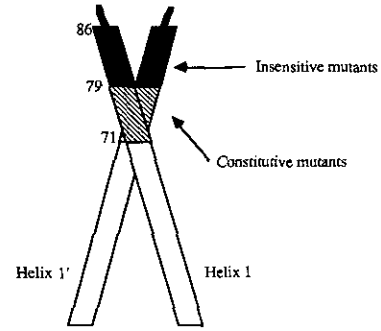

Figure 16. Schematic representation of the *E. coli* Trg receptor periplasmic domain subunit interface composed of helix 1 and helix 1′ based upon the aspartate receptor structure, depicting amino acid mutations that impair Trg signalling. Both sets of mutations reside on helix 1 (and helix 1′) that terminate at residue 86 (in the Trg numbering scheme) based upon comparison to the aspartate receptor crystal structure. The first set of mutations (residues 71 through 79) corresponds to the constitutively signalling or on phenotype, and are illustrated as the cross-hatched region. The second set of mutations (residues 79 through 86) corresponds to the inhibited signalling or off phenotype, and are illustrated as a blackened region.

We propose that residues 71 to 79, whose mutation leads to "constitutive signalling", are important constituents of the dimer interface of the periplasmic domain subunits of the Trg receptor. Perturbation of this interface may disturb the delicate interactions responsible for locking the receptor dimer into the off conformational state. Residues 79 to 86 are more exposed than those of the previous group, and are thus excellent candidates for being involved directly in binding galactose and ribose-binding proteins (Fig. 16). Mutations in this region interfere with ligand binding and give rise to the "insensitive" phenotype by disrupting the integrity of the protein binding site, consistent with this prediction. Additional evidence for the accuracy of this prediction is provided in the recent structural comparison of the galactose and ribose-binding proteins (Mowbray, 1992).

We thank B. Lynch, B. Stoddard and H. P. Biemann for helpful discussions and G. Hazelbauer, M. Manson, and M. Simon for providing experimental results prior to publication. Supported in part by NIH grants AI 30725 to S.H.K. and DK09765 to D.E.K., DOE (Director, Office of Energy Research, Office of Biological and Environmental Research, General Life Sciences Division under contract DE-AC03-76SF0098 to S.-H.K.), and the William M. Keck Foundation.

Atomic co-ordinates have been deposited with the Brookhaven Protein Data Bank under the accession number 1LIG.

References

Adler, J. (1966). Chemotaxis in bacteria. *Science*, **153**, 708–716.

Adler, J., Hazelbauer, G. L. & Dahl, M. M. (1973). Chemotaxis toward sugars in *Escherichia coli*. *J. Bacteriol.* **115**, 824–847.

Argos, P. M., Rossmann, M. G. & Johnson, J. E. (1977). A four-helical super-secondary structure. *Biochem. Biophys. Res. Commun.* **75**, 83–86.

Bollinger, J., Park, C., Harayama, S. & Hazelbauer, G. L. (1984). Structure of the Trg protein: homologies with and differences from other sensory transducers of *Escherichia coli*. *Proc. Nat. Acad. Sci., U.S.A.* **81**, 3287–3291.

Bourret, R. B., Hess, J. F., Borkovich, K. A., Pakula, A. A. & Simon, M. I. (1989). Protein phosphorylation in chemotaxis and two-component regulatory systems of bacteria. *J. Biol. Chem.* **264**, 7085–7088.

Bourret, R. B., Borkovich, K. A. & Simon, M. I. (1991). Signal transduction pathways involving protein phosphorylation in prokaryotes. *Annu. Rev. Biochem.* **60**, 401–441.

Brünger, A. (1990). *XPLOR 2.1: A system for crystallography and NMR*, Yale University.

Chothia, C., Levitt, M. & Richardson, D. (1977). Structure of proteins: Packing of α-helices and pleated sheets. *Proc. Nat. Acad. Sci., U.S.A.* **74**, 4130–4134.

Chothia, C., Levitt, M. & Richardson, D. (1981). Helix to helix packing in proteins. *J. Mol. Biol.* **145**, 215–250.

Chothia, C., Lesk, A. M., Dodson, G. G. & Hodgkin, D. C. (1983). Transmission of conformational change in insulin. *Nature (London)*, **302**, 500–505.

Claesson-Welsh, L., Eriksson, A., Moren, A., Severinsson, L., Ek, B., Ostman, A., Betsholtz, C. & Heldin, C. H. (1988). cDNA cloning and expression of a human platelet-derived growth factor (PDGF) receptor specific for B-chain-containing PDGF molecules. *Mol. Cell Biology* **8**, 3476–3486.

Cohen, C. & Parry, D. A. D. (1990). α-Helical coiled coils and bundles: how to design an α-helical protein. *Proteins*, **7**, 1–15.

Coussens, L., Van Beveren, C., Smith, D., Chen, E., Mitchell, R. L., Isacke, C. M., Verman, I. M. & Ullrich, A. (1986). Structural alteration of viral homologue of receptor proto-oncogene fms at carboxyl terminus. *Nature (London)*, **320**, 277–280.

Crick, F. H. C. (1953). The packing of α-helices: simple coiled-coils. *Acta Crystallogr.* **6**, 689–97.

de Vos, A. M., Ultsch, M. & Kossiakoff, A. A. (1992). Human growth hormone and extracellular domain of its receptor: crystal structure of the complex. *Science*, **255**, 306–312.

Falke, J. J. & Koshland, D. E., Jr (1987). Global flexibility in a sensory receptor: a site-directed cross-linking approach. *Science*, **237**, 1596–1600.

Falke, J. J., Dernburg, A. F., Sternberg, D. A., Zalkin, N., Milligan, D. L. & Koshland, D. E., Jr (1988). Structure of a bacterial sensory receptor: a site-directed sulfhydryl study. *J. Biol. Chem.* **263**, 14850–14858.

Garavito, R. M. & Picot, D. (1990). The art of crystallizing membrane proteins. *Methods: Compan. Methods Enzymol.* **1**, 57–69.

Gardina, P., Conway, C., Kossman, M. & Manson, M. (1992). aspartate and maltose-binding protein interact with adjacent sites in the Tar chemotactic signal transducer of *Escherichia coli*. *J. Bacteriol.* **174**, 1528–36.

Hanks, S. K., Quinn, A. M. & Hunter, T. (1988). The protein kinase family: conserved features and deduced phylogeny of the catalytic domains. *Science*, **241**, 42–52.

Harayama, S., Engstrom, P., Wolf-Watz, H., Iino, T. & Hazelbauer, G. L. (1982). Cloning of *trg*, a gene for a sensory transducer in *Escherichia coli*. *J. Bacteriol.* **152**, 372–383.

Higashi, T. (1989). The processing of diffraction data taken on a screenless Weissenberg camera for macromolecular crystallography. *J. Appl. Crystallogr.* **22**, 9–18.

Ignolia, T. D. & Koshland, D. E., Jr (1979). Response to a metal ion-citrate complex in bacterial sensing. *J. Bacteriol.* **140**, 798–804.

Imae, Y., Oosawa, K., Mizuno, T., Kihara, M. & Macnab, R. M. (1987). Phenol: a complex chemoaffector in bacterial chemotaxis. *J. Bacteriol.* **169**, 371–379.

Jancarik, J., Scott, W. G., Milligan, D. L., Koshland, D. E., Jr & Kim, S. H. (1991). Crystallization and preliminary X-ray diffraction study of the ligand-binding domain of the bacterial chemotaxis-mediating aspartate receptor of *Salmonella typhimurium*. *J. Mol. Biol.* **221**, 31–34.

Jones, T. A. (1978). A graphics model building and refinement system for macromolecules. *J. Appl. Crystallogr.* **11**, 268–272.

Koiwai, O. & Hayashi, H. (1979). Studies on bacterial chemotaxis. IV. Interaction of maltose receptor with a membrane-bound chemotaxis component. *J. Biochem.* **86**, 27–34.

Koshland, D. E., Jr (1988). Chemotaxis as a model second messenger system. *Biochemistry*, **27**, 5829–5834.

Kossmann, K., Wolff, C. & Manson, M. D. (1988). Maltose chemoreceptor of *Escherichia coli*: interaction of maltose-binding protein and the Tar signal transducer. *J. Bacteriol.* **170**, 4516–4521.

Kraulis, P. J. (1991). MOLSCRIPT: a program to produce both detailed and schematic plots of protein structures. *J. Appl. Crystallogr.* **24**, 946–950.

Krikos, A., Mutoh, N., Boyd, A. & Simon, M. I. (1983). Sensory transducers of *E. coli* are composed of discrete structural and functional domains. *Cell*, **33**, 615–622.

Lederberg, J. (1956). Linear inheritance in transduction clones. *Genetics*, **41**, 845–871.

Lee, L. & Imae, Y. (1990). Role of threonine residue 154 in ligand recognition of the Tar chemoreceptor in *Escherichia coli*. *J. Bacteriol.* **172**, 377–382.

Lee, B. & Richards, F. M. (1971). The interpretation of protein structures: estimation of static accessibility. *J. Mol. Biol.* **55**, 379–400.

Luzzati, P.V. (1952). Traitement statistique des erreurs dans la determination des structures cristallines. *Acta Crystallogr.* **5**, 802–810.

Lynch, B. A. & Koshland, D. E., Jr (1991). Disulfide crosslinking studies of the transmembrane regions of the aspartate sensory receptor of *Escherichia coli*. *Proc. Nat. Acad. Sci., U.S.A.* **88**, 10402–10406.

Lynch, B. A. & Koshland, D. E., Jr (1992). Structural similarities between the aspartate receptor of bacterial chemotaxis and the Trp repressor of *E. coli*: implications for transmembrane signalling. *FEBS Letters*, **307**, 3–9.

Macnab, R. M. (1987). Motility and chemotaxis. In Escherichia coli *and* Salmonella typhimurium: *Cellular and Molecular Biology* (Neidhardt, F. C., ed.), American Society for Microbiology, Washington, DC.

Macnab, R. M. & Koshland, D. E., Jr (1972). The gradient-sensing mechanism in bacterial chemotaxis. *Proc. Nat. Acad. Sci., U.S.A.* **69**, 2509–2512.

Manson, M. D., Boos, W., Bassford, P. J. & Rasmussen, B. A. (1985). Dependence of maltose transport and chemotaxis on the amount of maltose-binding protein. *J. Biol. Chem.* **260**, 9727–9733.

Milburn, M. V., Prive, G. G., Milligan, D. L., Scott, W. G., Yeh, J., Jancarik, J., Koshland, D. E., Jr & Kim, S. H. (1991). Three-dimensional structures of the ligand-binding domain of the bacterial aspartate receptor with and without a ligand. *Science*, **254**, 1342–1347.

Milligan, D. L. (1991). Ph.D. thesis. Structure and dynamics of the aspartate chemoreceptor. Department of Molecular and Cellular Biology, University of California, Berkeley, CA.

Milligan, D. L. & Koshland, D. E., Jr (1988). Site-directed cross-linking: establishing the dimeric structure of the aspartate receptor of bacterial chemotaxis. *J. Biol. Chem.* **263**, 6268–6275.

Milligan, D. L. & Koshland, D. E., Jr (1991). Intra-subunit signal transduction by the aspartate chemoreceptor. *Science*, **254**, 1651–1654.

Moe, G. R. & Koshland, D.E., Jr (1986). Transmembrane signalling through the aspartate receptor. In *Microbial Energy Transduction: Genetics, Structure and Function of Membrane Proteins* (Youvan, D. C. & Daldal, F., eds), pp. 163–168, Cold Spring Harbor Laboratory Press, Cold Spring Harbor, NY.

Moe, G. R., Bollag, G. E. & Koshland, D.E., Jr (1989). Transmembrane signaling by a chimera of the *Escherichia coli* aspartate receptor and the human insulin receptor. *Proc. Nat. Acad. Sci., U.S.A.* **86**, 5683–5687.

Molecular Structure Corp. (1991). R-Axis II software, based on Rossmann (1979).

Mowbray, S. L. (1992). Ribose and glucose-galactose receptors: competitors in bacterial chemotaxis. *J. Mol. Biol.* **227**, 418–440.

Mowbray, S. L. & Koshland, D. E., Jr (1987). Additive and independent responses in a single receptor: aspartate and maltose stimuli on the Tar protein. *Cell*, **50**, 171–180.

Mowbray, S. L. & Koshland, D. E., Jr (1990). Mutations in the aspartate receptor of *Escherichia coli* which affect aspartate binding. *J. Biol. Chem.* **265**, 15638–15643.

Mowbray, S. L., Foster, D. L. & Koshland, D. E., Jr (1985). Proteolytic fragments identified with domains of the aspartate chemoreceptor. *J. Biol. Chem.* **260**, 11711–11718.

O'Shea, E. K., Klemm, J. D., Kim, P. S. & Alber, T. (1991). X-ray structure of the GCN4 leucine zipper, a two-stranded parallel coiled-coil. *Science*, **254**, 539–544.

Pakula, A. A. & Simon, M. I. (1992). Determination of transmembrane protein structure by disulfide cross-linking: the *E. coli* Tar receptor. *Proc. Nat. Acad. Sci., U.S.A.* **89**, 4144–4148.

Parada, L. F. (1991). The *trk* proto-oncogene product: a signal transducing receptor for nerve growth factor. *Science*, **252**, 554–557.

Ramachandran, G. N. & Sassiekharan, V. (1968). Conformation of polypeptides and proteins. *Advan. Protein Chem.* **28**, 283–437.

Richarme, G. (1982). Interaction of the maltose-binding protein with membrane vesicles of *Escherichia coli*. *J. Bacteriol.* **149**, 662–667.

Rossmann, M. J. (1979). Processing oscillation diffraction data for very large unit cells with an automatic convolution technique and profile fitting. *J. Appl. Crystallogr.* **12**, 225–238.

Russo. A. F. & Koshland, D. E, Jr (1983). Separation of signal transduction and adaptation functions of the aspartate receptor in bacterial sensing. *Science*, **220**, 1016–1020.

Scott, W. G. (1992). Ph.D. thesis. Three-dimensional structures of the ligand-binding domain of the aspartate receptor. Department of Chemistry, University of California, Berkeley, CA.

Segall, J. E., Block, S. M. & Berg, H. C. (1986). Temporal comparisons in bacterial chemotaxis. *Proc. Nat. Acad. Sci., U.S.A.* **83**, 8987–8991.

Sim, G. A. (1960). A note on the heavy-atom method. *Acta Crystallogr.* **13**, 511–512.

Steigemann, W. (1982). *PROTEIN: A package of crystallography programs for analysis of proteins*, Max Planck Institute for Biochemistry, Martinsried, Germany.

Stock, J. B., Stock, A. M. & Mottonen, J. M. (1990). Signal transduction in bacteria. *Nature (London)*, **344**, 395–400.

Stock, J. B., Surette, M. G., McCleary, W. R. & Stock, A. M. (1992). Signal transduction in bacterial chemotaxis. *J. Biol. Chem.* **267**, 19753–19756.

Stoddard, B. L. & Koshland, D. E., Jr (1992). Prediction of the structure of a receptor protein complex using a binary docking method. *Nature (London)*, **358**, 774–776.

Strange, P. G. & Koshland, D.E., Jr (1976). Receptor interactions in a signalling system: competition between ribose receptor and galactose receptor in the chemotaxis response. *Proc. Nat. Acad. Sci., U.S.A.* **73**, 762–766.

Terwilliger, T. C., Wang, J. Y. & Koshland, D. E., Jr (1986). Surface structure recognized for covalent modification of the asparate receptor in chemotaxis. *Proc. Nat. Acad. Sci., U.S.A.* **83**, 6707–6710.

Terwilliger, T. C., Kim, S. H. & Eisenberg, D. (1987). Generalized method of determining heavy-atom positions using the difference Patterson function. *Acta Crystallogr. sect. A*, **43**, 1–5.

Tso, W. W. & Adler, J. (1974). Negative chemotaxis in *Escherichia coli*. *J. Bacteriol.* **118**, 560–576.

Ullrich, A. & Schlessinger, J. (1990). Signal transduction by receptors with tyrosine kinase activity. *Cell*, **61**, 203–212.

Ullrich, A., Coussens, L., Hayflick, J. S., Dull, T. J., Gray, A., Tam, A. W., Lee, J., Yarden, Y., Libermann, T. A., Schlessinger, J., Downward, J., Mayes, E. L. V., Wittle, N., Waterfield, M. D. & Seeburg, P. H. (1984). Human epidermal growth factor receptor cDNA sequence and aberrant expression of the amplified gene in A431 epidermoid carcinoma cells. *Nature (London)*, **309**, 418–425.

Ullrich, A., Bell, J. R., Chen, E. Y., Herrera, R., Petruzzelli, L. M., Dull, T. J., Gray, A., Coussens, L., Lio, Y. C., Tsubokawa, M., Manson, A., Seeburg, P. H., Grunfeld, C., Rosen, O. M. & Ramachandran, J. (1985). Human insulin receptor and its relationship to the tyrosine kinase family of oncogenes. *Nature (London)*, **313**, 756–761.

Ullrich, A., Gray, A., Tam, A. W., Yang-Feng, T., Tsubokawa, M., Collins, C., Henzel, W., Le Bon, T. Kathuria, S., Chen, E., Jacobs, S. Francke, U., Ramachandran, J. & Fujita-Yamaguchi, Y. (1986). Insulin-like growth factor I receptor primary struc-

ture: comparison with insulin receptor suggests structural determinants that define functional specificity. *EMBO J.* **5**, 2503–2512.

Weber, P. C. & Salemme, F. R. (1980). Structural and functional diversity in 4-α-helical proteins. *Nature (London)*, **287**, 82–85.

Weis, R. M. & Koshland, D. E., Jr (1988). Reversible receptor methylation is essential for normal chemotaxis of *Escherichia coli* in gradients of aspartic acid. *Proc. Nat. Acad. Sci., U.S.A.* **85**, 83–87.

Wolff, C. & Parkinson, J. S. (1988). Aspartate taxis mutants of the *Escherichia coli* Tar chemoreceptor. *J. Bacteriol.* **170**, 4509–4515.

Yaghmai, R., & Hazelbauer, G. L. (1992). Ligand occupancy mimicked by single residue substitutions in a receptor: transmembrane signalling induced by mutation. *Proc. Nat. Acad. Sci., U.S.A.* **8**. 7890–7894.

Yarden, Y. & Ullrich, A. (1988). Growth factor receptor tyrosine kinases. *Annu. Rev. Biochem.* **57**, 443–478.

Edited by P. E. Wright